arXiv:1611.03878v1 [astro-ph.HE] 11 Nov 2016

New High-z Fermi BL Lacs with the Photometric Dropout Technique

A. Kaur[1], A. Rau[2], M. Ajello[1], J. Greiner[2], D. H. Hartmann[1], V. S. Paliya[1],A. Domínguez[3], J. Bolmer[2,4], P. Schady[2]

[1]*Department of Physics and Astronomy, Clemson University, SC 29634-0978, U.S.A.*

akaur@g.clemson.edu

[2]*Max-Planck-Institut für extraterrestrische Physik, Giessenbachstraße 1, 85748 Garching, Germany*

[3]*Grupo de Altas Energías, Universidad Complutense, E-28040 Madrid, Spain*

and

[4]*European Southern Observatory, Alonso de Córdova 3107, Vitacura, Casilla 19001, Santiago 19, Chile*

ABSTRACT

Determining redshifts for BL Lacertae (BL Lac) objects using the traditional spectroscopic method is challenging due to the absence of strong emission lines in their optical spectra. We employ the photometric dropout technique to determine redshifts for this class of blazars using the combined 13 broad-band filters from *Swift*-UVOT and the multi-channel imager GROND at the MPG 2.2 m telescope at ESO's La Silla Observatory. The wavelength range covered by these 13 filters extends from far ultraviolet to the near-Infrared. We report results on 40 new Fermi detected BL Lacs with the photometric redshifts determinations for 5 sources, with 3FGL J1918.2-4110 being the most distant in our sample at z=2.16. Reliable upper limits are provided for 20 sources in this sample. Using the highest energy photons for these Fermi-LAT sources, we evaluate the consistency with the Gamma-ray horizon due to the extragalactic background light.

Subject headings: (galaxies:) BL Lacertae objects: general — galaxies: active — gamma rays: diffuse background

1. Introduction

Blazars represent a class of active galactic nuclei (AGNs) with relativistic jets pointing along our line of sight (Blandford & Rees 1978). Their spectral energy distribution (SED) exhibits two characteristic broad bumps, which are attributed to synchrotron emission at the lower energies (Infrared to X-ray) and synchrotron self Compton at the higher energies (X-ray to γ-rays, e.g. Maraschi et al. 1994). On the basis of their optical spectroscopic characteristics, blazars can be further classified into two types : Flat Spectrum Radio Quasars (FSRQs), characterized by broad emission lines and BL Lacertae objects (BL Lacs), with no or at best weak emission lines (equivalent width < 5 Å, Urry & Padovani 1995). Furthermore, another classification scheme for blazars was introduced by Abdo et al. (2010) based on the location of their synchrotron peak frequency, ν_{pk}^{sy}. The authors subdivided these objects into three classes: high-synchrotron-peaked blazars (HSP) for $\nu_{pk}^{sy} > 10^{15}$ Hz, intermediate-synchrotron-peak (ISP) for 10^{14} Hz $< \nu_{pk}^{sy} < 10^{15}$ Hz and low-synchrotron-peak (LSP) for $\nu_{pk}^{sy} < 10^{14}$ Hz. Most of the FSRQs fall in the LSP category, but half the population of BL Lacs display peak synchrotron frequencies $> 10^{15}$ Hz (Ackermann et al. 2015). These high values of ν_{pk}^{sy} imply the presence of relativistic multi-TeV electrons, therefore making BL Lacs very bright γ-ray sources with substantial emission above 10 GeV (Ackermann et al. 2013).

Blazars play an important role in the study of the Extragalactic Background Light (EBL), which represents the integrated light from all the stars and other compact objects since the re-ionization epoch. The photons from blazars are attenuated by EBL photons through production of electron-positron pairs, which imprint a characteristic signature in the spectra of these γ-ray sources (Stecker et al. 1992). This feature in blazar spectra enables us to constrain the EBL and

its evolution with cosmic time (Aharonian et al. 2006; Ackermann et al. 2012; Domínguez et al. 2013). In the case of FSRQs, the presence of broad emission lines implies the presence of a disk, whose UV radiation field could attenuate γ-ray photons, thereby making it a challenging task to differentiate the attenuation signal from the EBL photons from the circumnuclear one. On the other hand, absence of broad emission lines in BL Lacs in addition to the abundance of photons above 10 GeV render them the perfect class of blazars to explore the EBL (Domínguez & Ajello 2015). To enable such studies, redshift measurements for these sources are essential. In particular, high redshift BL Lacs are critical for probing the EBL, since the strength of the attenuation increases with redshift. Moreover, high-z blazars are crucial for testing the EBL evolution, which at present is poorly constrained. Estimating redshifts of BL Lacs in the traditional spectroscopic way is yet another challenge, because of the weakness, or even absence of lines (Shaw et al. 2013). Rau et al. (2012) initiated a program to determine redshifts for BL Lac sources via a photometric technique. The underlying principle for this photometric redshift (photo-z) determination is based on the absorption of UV photons by neutral hydrogen along the line of sight, which absorbs photons bluewards of the Lyman limit. This leads to a dropout in the flux at the Lyman limit whose position in the SED can be used to determine the photo-z. This approach was applied by Rau et al. (2012) for a sample of 103 blazars.

The immediate aim of this study is to determine photo-zs of high-z ($z > 1.3$, which is the lower limit measurable with this method) BL Lacs to increase the sample in the important high redshift regime. Only 19 BL Lacs with $z > 1.3$ are known, of which 13 are reported in the third catalog of Fermi-detected AGNs (3LAC, Ackermann et al. (2015)). A total of 9 BL Lacs were reported in Rau et al. (2012), of which three sources are provided among the 13 in the 3LAC catalog. Therefore, Rau et al. (2012) provided 6 new high-z BL Lacs with the photometric technique.

The outline of this paper is as follows: Section 2 explains the details of observations. The data analysis procedure is explained in section 3. The resulting high-z BL Lacs parameters are reported in section 4 and the interpretation of our results is presented in section 5. A flat ΛCDM cosmological model with H_0=71 km s^{-1} Mpc^{-1}, Ω_m=0.27 and Ω_Λ =0.73 was adopted for all the calculations in this work in order to be consistent with the work presented in Finke (2013).

2. Observations

2.1. Sample Selection

Our sample was selected from sources classified as BL Lacs in the third catalog of Fermi detected sources (3FGL, Acero et al. 2015) without a measured redshift. The selection procedure was based on two main criteria, one being that only sources with Declination $< 25^\circ$ were chosen in order to accommodate the visibility from the ground based telescope, situated in Chile. The second selection criterion was the minimization of the Galactic foreground reddening, ensured by selecting objects away from the Galactic Plane ($|b| > 10$ $^\circ$). Here we report on the 40 sources observed so far whose basic properties are presented in Table 1.

2.2. Facilities

The *Swift* satellite (Gehrels et al. 2004) and MPG 2.2 m telescope at ESO La Silla, Chile were employed for conducting the observations. All sources were observed in 13 filters; (*uvw2, uvm2, uvw1, u, b, v*) of *Swift*-UVOT (The Ultraviolet and Optical Telescope, Roming et al. 2005) and 7 optical-IR filters ($g', r', i', z', J, H, K_s$) of GROND (Gamma-Ray Optical/Near-infrared Detector, Greiner et al. 2008). The resulting 13-filter SED covers a wavelength range of 1600 Å- 20000 Å. The main advantage of using the overlap of two filters : g' from GROND and *b* from UVOT is to cross-calibrate the two instruments for the combined data analysis.

2.3. Observing Strategy

GROND observations were performed as close to the *Swift* observations as possible. While truly simultaneous observations were rarely feasible due to ground visibility constraints, both instruments often observed within 1-2 days of each other. *Swift*-UVOT observed in each of its six filters in sequence, while GROND conducted observations in all the 7 filters, simultaneously, which is very crucial for blazars, due to their variable nature. The typical integration times for *Swift* were 100 s each in *u, b, v* and 200, 240 and 400 s in *uvw1, uvm2, uvw2*, respectively, although the exposure times changed based on the brightness of each object. A typical GROND observation had an integration time of $\sim$ 2 min in g', r', i', z' and $\sim$ 4.0 min in J, H, K_s.

3. Data Analysis

3.1. *Swift-UVOT*

Swift data were processed through the standard UVOT pipeline procedure (Poole et al. 2007) in order to remove the bad pixels, to flat-field and to correct for the system response. The magnitude extraction per filter was performed with the UVOT task, `UVOTMAGHIST`. A circular region was selected for the aperture extraction with variable radius in order to maximize the signal to noise ratio. The resulting magnitudes in each filter were corrected for Galactic extinction, utilizing table 5 presented in Kataoka et al. (2008). The final magnitudes were converted to the AB system and the results are presented in Table 2.

3.2. GROND

The data reduction procedure for GROND is described in detail in Krühler et al. (2008), and here it is only mentioned briefly. The point spread function (PSF) photometric technique was used for g', r', i', z' filters, whereas due to the undersampled PSF in the near infrared, the standard aperture extraction technique was applied for *J, H,* K_s photometry. The 4 optical filters were calibrated with the stars in the SDSS Data Release 8 (Aihara et al. 2011), which provides the final magnitudes in the AB system. 2MASS stars (Skrutskie et al. 2006) were employed for calibration of the near-IR filters. The correction for the Galactic foreground extinction was performed with measurements in Schlafly & Finkbeiner (2011). The resulting data were converted to the AB system (Table 3).

3.3. Variability Correction

Blazars, in general, exhibit emission which varies on time scale of a few minutes to years. This variability can have a significant impact on the redshift determination via the photometric technique. GROND data are not affected by intrinsic variability as the observations are performed in all seven filters simultaneously. However, since *Swift*-UVOT cycles through every filter, in addition to the non-simultaneous GROND-*Swift* observations, these variations in the emission could add to the existing uncertainties. Rau et al. (2012) established that the inherent blazar variability introduces a systematic uncertainty of Δ m = 0.1 mag for each UVOT filter. The other important factor to consider is that the total SED is obtained by combining the UVOT and GROND data, which are two different instruments, which thus need to be calibrated against each other. Krühler et al. (2011) performed this task by combining *Swift*-UVOT and GROND filter curves, utilizing their spectral overlap and established the following calibration relationship:

$$b - g' = 0.15\,(g' - r') + 0.03\,(g' - r')^2 \quad (1)$$

This equation is based on the assumption that a BL Lac SED is represented by a power law and that its slope does not change over the UV-IR regime. This relation which is valid for -1 $\leq (g' - r') \leq$ 2 was applied to all the UVOT filters before SED fitting. The UV-Opt-IR SED of BL Lacs is thought to be dominated by non-thermal synchrotron emission. It can be modeled over the wavelength interval used here as a powerlaw spectrum. Our 13 band photometry covers this energy regime of the SED of a BL Lac, and moreover the absence of any broad lines makes this approximation valid in particular for these kind of blazars. In addition, stellar templates were fitted to these sources to check for non-powerlaw behavior as explained in the next section.

3.4. SED fitting

The `LePhare v.2.2` program [1] (Arnouts et al. 1999; Ilbert et al. 2006) was employed to determine the photometric redshifts for these objects. This program evaluates the difference between the observational and theoretical data based on χ^2 statistic. We selected three separate template libraries to fit the data, independently. Our first library is comprised of 60 powerlaw SED templates of the form $F_\lambda \propto \lambda^{-\beta}$, such that β ranged from 0 to 3 in steps of 0.05, under the assumption that the UV-Optical-NearInfrared regime for BL Lacs can be fit with a single power-law template. In addition, a library of galaxies and galaxy/AGN hybrids (Salvato et al. 2009, 2011) as well as a stellar library using templates from Pickles (1998), Bohlin et al. (1995) and Chabrier et al. (2000) were used. The results from the first two libraries are presented in Table 4. None of our SEDs required a contribution from the stellar libraries.

4. Results

The results of SED fitting for 40 sources are presented in Table 4. The reliability of our photometric results was determined by Monte Carlo simula-

[1] http://www.cfht.hawaii.edu/ arnouts/lephare.html

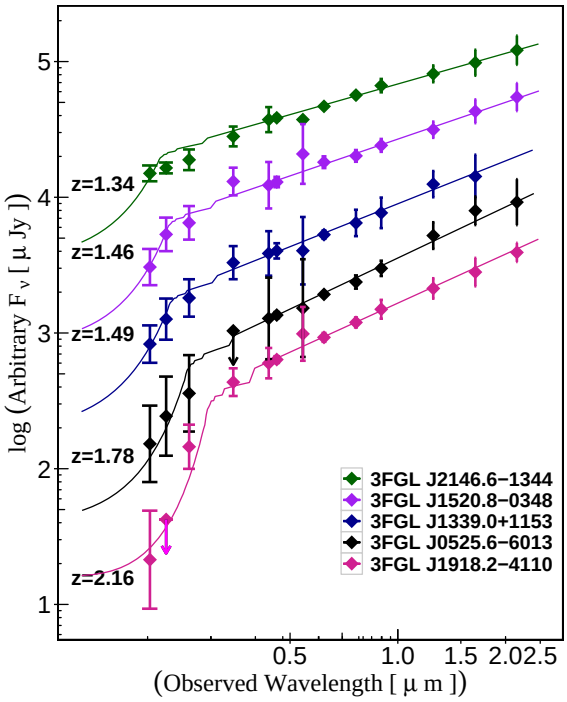

Fig. 1.— The $Swift$-UVOT + GROND spectral energy distribution for 5 high-z BL Lacs with determined redshifts. The lines show the power law template fits for each source as described in Section 3.4. The details of these fits are provided in Table 4. The arrows correspond to the upper limits for the measured flux.

tions performed in Rau et al. (2012), where 27000 test SEDs were simulated with β ranging from 0.5-2.0 and redshifts 0 to 4. These SEDs were supplied to `LePhare` to calculate the redshifts and were then compared to the input values. The authors concluded that for sources with simulated redshifts, $z_{sim} > 1.2$, the photometric redshift reproduced the input value within an accuracy of $|\Delta z(1 + z_{sim})| < 0.15$. In addition, a more quantitative selection procedure was applied, which was based on a quantity, $P_z = \int f(z)dz$ at $z_{phot} \pm 0.1(1 + z_{phot})$, the integral of the probability distribution function. This quantity describes the probability that the redshift of a source is within a factor of 0.1(1+z) of the best fit value. Measurements with $P_z > 90\%$ were considered reliable photometric redshifts. We apply both selection criteria defined above to our SED fitting, which resulted in determining photometric redshifts for 5 sources and establishing upper limits for 20 of them, which is presented in Table 4. The $Swift$-UVOT and GROND spectral energy distributions for the new 5 high-z sources, i.e., 3FGL J0525.6-6013, 3FGL J1339.0+1153, 3FGL J1520.8-0348, 3FGL J1918.2-4110, 3FGL J2146.6-1344 is shown are Figure 1.

5. Discussion

Ackermann et al. (2015) reported 604 BL Lacs out of which 326 sources have redshift measurements of which only 13 with high-z (z $>$ 1.3). 3 of these sources were reported among the 9 high-z BL Lacs by Rau et al. (2012) utilizing the photometric redshift technique. Our study is a continuation of Rau et al. (2012), who calculate the redshifts for BL Lacs with photometric technique, which increases the sample size by $\sim$ 30% by finding 5 BL Lacs at $z > 1.3$ from our sample of 40 sources. $\sim$ 50% of the total number of 24 known high-z BL Lacs (5 from this work and 6 from Rau et al. (2012)'s work) are determined by the photo-z method. A comparison between the spectroscopic and photometric redshift determinations for $z > 1.3$ BL Lacs is presented in Figure 2. As seen in this figure, both approaches are consistent with each other. The spectroscopic redshift for the source, 3FGL J1312.5-2155 has been determined by using the absorption features, i.e., C IV and Mg II (Ryabinkov et al. 2003), which could possibly imply a lower limit. This comparison demonstrates that our photometric campaign is an efficient way to uncover rare high-redshift BL Lacs.

5.1. Blazar Sequence

"Blazar Sequence" is a scheme, which suggests the existence of a unified model to represent all classes of blazars. Several authors e.g. Maraschi et al. (1995), Sambruna et al. (1996), Fossati et al. (1998) proposed this unification idea through observed SEDs for blazars. These authors concluded that the blazar phenomenon is primarily governed by the total luminosity, which is the best indicator for determining the physical properties as well as the radiation mechanisms in these sources. Fossati et al. (1998) noticed several anti-correlations e.g. ν_{sy}^{pk} and luminosity at this peak (L_{sy}^{pk}), ν_{sy}^{pk} and the Compton Dominance (CD), and the γ-ray photon index (Γ_γ). These results indicate that the blazar family lined up on a sequence where more luminous blazars had lower synchrotron peak frequencies, but dominant γ-ray emission (i.e. CD $>$ 1), generally the case for powerful FSRQs. On the other hand, the less luminous, high-peaked sources (typically BL Lac objects) have CD $\lesssim$ 1. In other words, blazar sequence

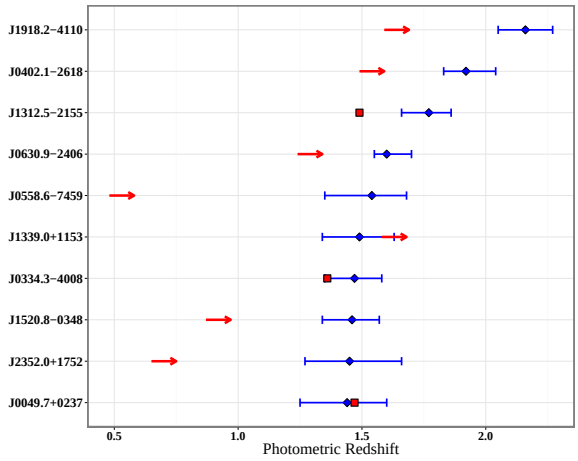

Fig. 2.— Spectroscopic (*red* filled squares) vs photometric redshifts (*blue* filled diamonds) comparison for sources with $z > 1.3$. The red arrows represent the spectroscopic lower limits for these sources. The confirmed spectroscopic redshifts were extracted from 3 LAC data (Ackermann et al. 2015) and the lower limits were obtained from Shaw et al. (2013). The photometric data were obtained from Rau et al. (2012) and this work. The y-axis naming convention follows from the 3FGL catalog.

predicts the non-existence of high frequency peaked, highly luminous BL Lac objects. A theoretical justification of these correlations are discussed in Ghisellini et al. (1998).

The concept of a Blazar sequence is an interesting but still debated idea (e.g. Padovani et al. (2012); Ghisellini et al. (2012)). The motivation here is to test how the new high-redshift BL Lacs presented in this study fit in the proposed blazar sequence. We utilize the 3LAC (Ackermann et al. 2015) catalog to extract relevant SED parameters, e.g., ν_{sy}^{pk}, $(\nu F_\nu)_{sy}^{pk}$, Compton Dominance and γ-ray photon index, for all the blazars present in 3LAC data. $(\nu F_\nu)_{sy}^{pk}$ was calculated using equation 4 in Abdo et al. (2010) assuming a flat spectrum for blazars in the radio regime, where the radio flux was obtained from Table 8 in Ackermann et al. (2015). All the other parameters were extracted from Table 4 in Ackermann et al. (2015). For those sources in our sample for which CD values were not provided, we calculated them with an online SED fitting tool[1]. We calculate luminosities at the peak synchrotron frequencies as they would appear in their rest frame. The obtained parameters are presented in Figure 3, 4 and 5. It should be noted that only blazars with known redshifts are plotted in these figures. As can be seen in Figure 3, the five high redshift BL Lac objects (shown with *yellow* squares) tend to occupy the high L_{sy}^{pk}, and a relatively high ν_{sy}^{pk} region among the known blazar population. We find that all of our high-z BL Lacs are consistent with the known anti-correlation of CD and ν_{sy}^{pk} (see Figure 4) with $CD < 1$ for all the five high-z BL Lacs, as generally seen in this class of blazars. These findings are in agreement with the theoretical model of Finke (2013) which suggests the existence of sources with high ν_{sy}^{pk} and high L_{sy}^{pk} but having a CD value less than unity. Furthermore, these objects are hard γ-ray spectrum sources and we do not find any exception when placed in the γ-ray photon index vs. ν_{sy}^{pk} diagram (Figure 5).

[1] http://tools.asdc.asi.it/SED/

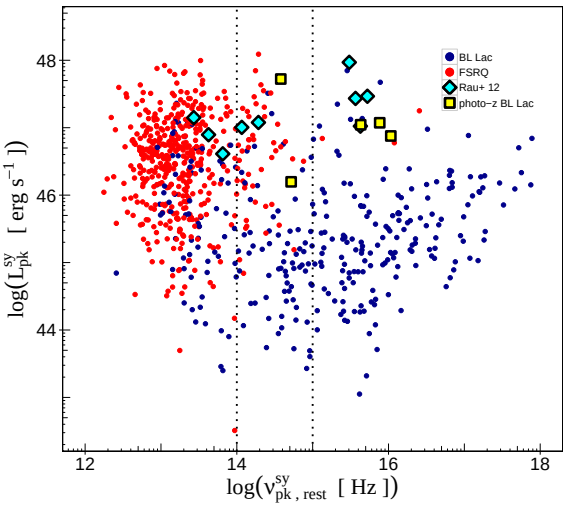

Fig. 3.— The peak synchrotron frequency in the rest frame (ν_{sy}^{pk}) vs the peak synchrotron luminosity (L_{sy}^{pk}). *Yellow* squares represent 5 new BL Lacs with $z > 1.3$, *cyan* diamonds are all the BL Lacs from Rau et al. (2012) (including the ones with known redshift via spectroscopic method), *blue* and *red* filled circles show BL Lacs and FSRQs, respectively in the 3LAC data. The vertical dashed lines show the divide between the LSP ($\nu_{sy}^{pk} < 10^{14}$ [Hz]), ISP, (10^{14} [Hz] $< \nu_{sy}^{pk} < 10^{15}$ [Hz]) and HSP ($\nu_{sy}^{pk} > 10^{15}$) BL Lacs. Note that only blazars with known redshifts are displayed here.

5.2. Fermi Blazar Divide

Ghisellini et al. (2009) utilized ∼100 blazars from the first 3-month survey of *Fermi*-LAT data (Abdo et al. 2009) and noticed a division between FSRQs and BL Lacs by comparing their γ-ray spectral indices (Γ_γ) to the γ-ray luminosities (L_γ). These observations revealed that BL Lacs exhibited harder spectra

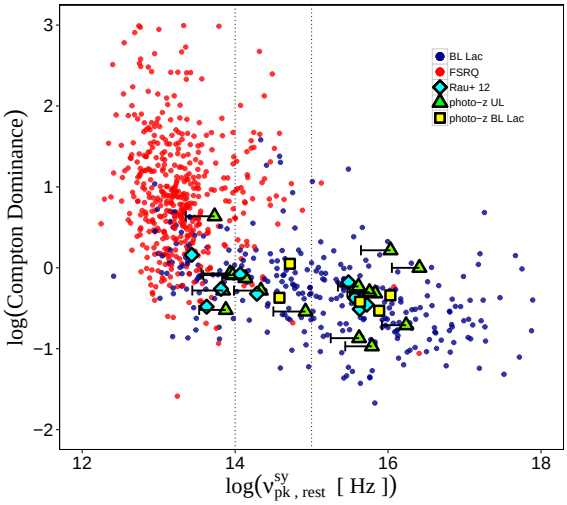

Fig. 4.— The relationship between the Compton Dominance and $\nu_{sy}^{\rm pk}$. The color scheme for data points follows from Figure 3. The *green* triangles represents 20 sources from our sample with upper limits for photo-zs. The 'UL' represents the BL Lacs with upper limits for photometric redshifts. The *black* horizontal bars represent the $\nu_{sy}^{\rm pk}$ with redshift range from zero to the upper limit provided in this work.

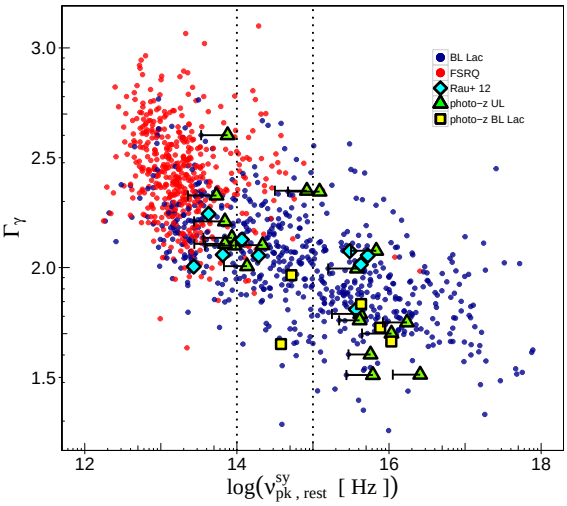

Fig. 5.— The correlation between the γ-ray photon index and the redshift corrected peak synchrotron frequency for all the blazars. The *black* horizontal bars represent the $\nu_{sy}^{\rm pk}$ with redshift range from zero to the upper limit provided in this work. The color scheme for different datasets follows from Figure 3. Please note that the γ-ray photon indices have not been corrected for the EBL absorption

.

($\Gamma_\gamma \lesssim 2.2$) and were less luminous ($L_\gamma \lesssim 10^{47}$ erg s^{-1}) than FSRQs. It was suggested that this "Fermi Blazar Divide" could be interpreted primarily based on the different mass accretion rates with FSRQs having high accretion rates.

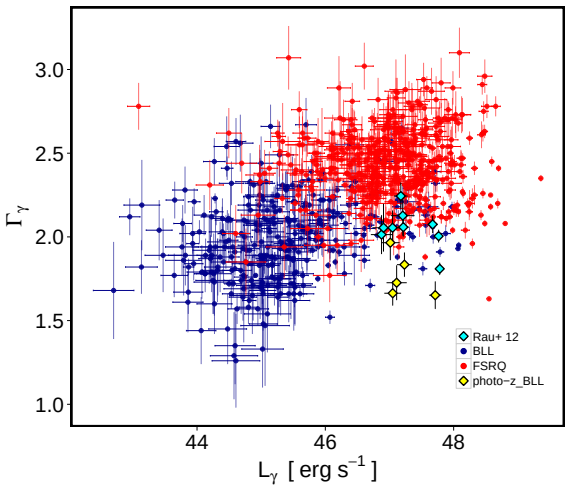

Fig. 6.— The correlation between the γ-ray luminosity (0.1-100 GeV) and the spectral index. The color scheme follows from Figure 3. Please note that the γ-ray photon indices have not been corrected for the EBL absorption

.

Moreover, this division between two groups of blazars on Γ_γ - L_γ plane has been discussed by various authors, e.g., Padovani et al. (2012), Ghisellini et al. (2012). The former authors noticed high L_γ and hard Γ_γ for some of the BL Lacs from Rau et al. (2012), which was argued against by the latter suggesting that although these BL Lacs fall into the higher end of Γ_γ - L_γ plane, yet they are consistent with the separation of two populations. In particular, Ghisellini et al. (2012) proposed that the emission region in these sources may lie outside the broad line region (BLR) and therefore the resultant SEDs are similar to BL Lacs. In other words, such objects are 'blue' FSRQs with the broad emission lines in their optical spectra are swamped by high level of synchrotron emission.

In Figure 6, we show the variation of L_γ as a function of Γ_γ for 3LAC blazars. In this diagram, we also show high-z BL Lacs obtained in this work and by Rau et al. (2012). The L_γ for all these sources were calculated using equation 1 in Ghisellini et al. (2009). Interestingly, as can be seen in Figure 6, all the five high-z BL Lacs have a hard Γ_γ (< 2.0) and their γ-ray luminosities are $\gtrsim 10^{47}$ erg s^{-1}. Now, following Sbarrato

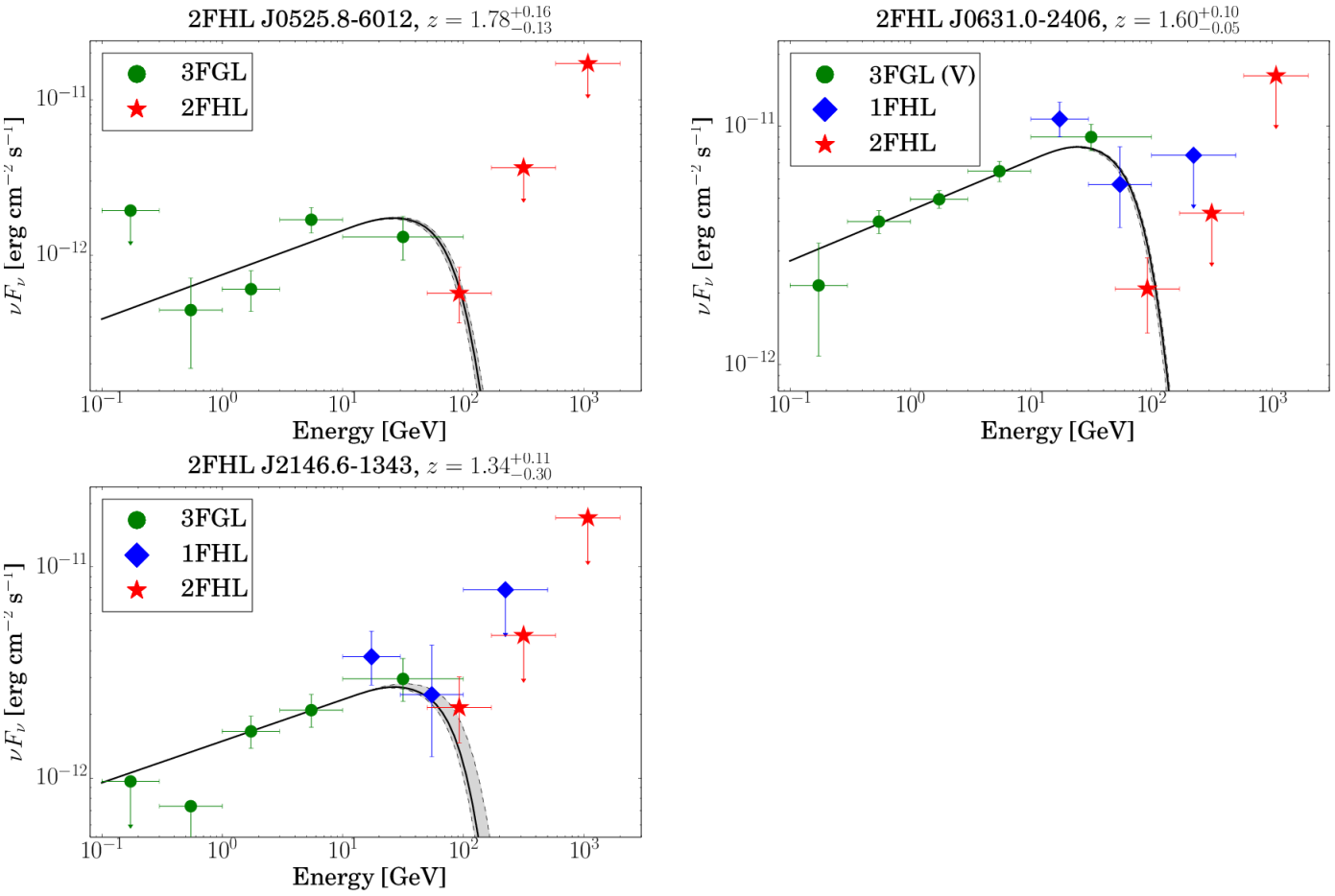

Fig. 7.— Spectral energy distributions of SUMSS J052542−601341, CRATES J0630−2406, and 1FGL J2146.6−134 obtained combining data reported in the 3FGL, 1FHL and 2FHL catalogs (Acero et al. 2015; Ackermann et al. 2013, 2016). The black line is a fit to the 3FHL data with a power law that is absorbed by the EBL using the model of Domínguez et al. (2011). The gray area at high energy denotes the uncertainty in the source attenuation (and correspondingly in the source flux) due to the uncertain redshift.

et al. (2012), we have

$$L_{\rm BLR} \sim 4 L_\gamma^{0.93} \quad (2)$$

where $L_{\rm BLR}$ is the BLR luminosity. This indicates that for $L_\gamma \sim 1 \times 10^{47}$ erg s^{-1}, we have $L_{\rm BLR} \sim 2 \times 10^{44}$ erg $^{-1}$. Assuming a fraction 10% of the disk luminosity is reprocessed by the BLR, the disk luminosity is $\sim 2 \times 10^{45}$ erg s^{-1}. Since there is no estimate of the central black hole mass available in the literature for the five high-z BL Lacs, we assume an average value of $5 \times 10^8\ M_\odot$ (e.g., Sbarrato et al. 2012).

This assumption implies $L_{\rm disk}/L_{\rm Edd} \sim 0.03$, which makes their accretion disk radiatively efficient, similar to what is typically observed in powerful FSRQs. However, these quantities should be considered with some caution due to underlying assumptions (e.g., Sbarrato et al. 2012; Ghisellini et al. 2012) and we defer to a future multi-wavelength study for a more detailed discussion. Furthermore, although the L_γ of these BL Lac objects appears to be similar to FSRQs, yet they are consistent with a separation in the γ-ray photon index alone, a property that has been established and known since EGRET and it is more robust against the redshifts completeness of the redshift population (e.g. Hartman et al. 1999; Venters & Pavlidou 2007).

5.3. The Extragalactic Background Light

Increasing the sample size of high-z BL Lacs is particularly important for probing the EBL , and to better understand the cosmic evolution of the blazar population (Ajello et al. 2012). Photons from sources at z >1.3 and energy above 50 GeV have a probability > 25 % of interacting with the photons of the UV-optical component of the EBL that leads to the generation of an electron-positron pair. For this reason, we looked into which source of the entire photo-z sample (5 sources from this paper and 6 from Rau et al. 2012) was also reported in the 2FHL catalog of *Fermi*-LAT sources detected above 50 GeV (Ackermann et al. 2016). We found three; 1FGL J2146.6−134, CRATES J0630−2406 and SUMSS J052542−601341. Their highest energy photons at 81 GeV, 83 GeV, and 71 GeV, respectively (reported in Ackermann et al. 2016) allow us to probe the cosmic γ-ray horizon (i.e. the distance at which $\tau_{\gamma\gamma} = 1$, e.g. Domínguez et al. 2013). Figure 8 shows that those photons are consistent with the γ-ray horizon in the EBL model developed by Domínguez et al. (2011). It is important to realize that these high-z sources provide a valuable constraint on the γ-ray horizon in a region where the sources are scarce.

Figure 7 shows the γ-ray SED of 1FGL J2146.6−134, CRATES J0630−2406 and SUMSS J052542−601341 obtained combining 3FGL, 1FHL and 2FHL data (Acero et al. 2015; Ackermann et al. 2013, 2016). For each source, we fitted a power law to the 3FGL data and applied to it EBL absorption (in the form $e^{-\tau(E,z)}$) adopting the Domínguez et al. (2011) model and taking the redshift uncertainty into account. All these sources exhibit hard spectra with photon spectral indices of $\Gamma \approx 1.8$, similar to the one of Mrk 421, but belonging to objects that are much farther away. The redshift uncertainty produces a negligible effect in the expected source flux at $z \gtrsim 1.5$. As such one may use BL Lacs with photo-z estimates to constrain the EBL in the same way as BL Lacs with spectroscopic redshift have been used in Ackermann et al. (2012).

Figs. 8 and 7 show that the γ-ray horizon is for $z \gtrsim 1.5$ is at energy $\lesssim$100 GeV: i.e. well in the *Fermi*-LAT band and well constrained by the first energy bin of the 2FHL catalog. For two out of three sources the flux is reduced by a factor $\gtrsim$5 with respect to the unabsorbed flux.

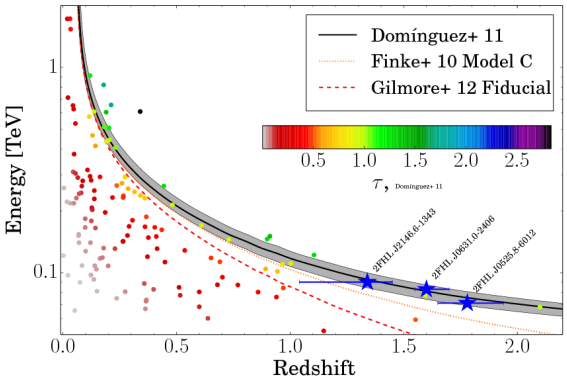

Fig. 8.— A plot of the highest energy of photons from sources (with E > 50 GeV) vs. their redshift. The colors of different sources imply their corresponding optical depth (τ) values (see colorbar. Various estimates of the cosmic γ-ray horizon, obtained from the EBL models by Finke et al. (2010)(dotted orange line), Domínguez et al. (2011) (solid black line, with its uncertainties as a shaded band) and Gilmore et al. (2011) (dashed red line) are plotted for comparison. The highest energy photons from three of the high-z sources from our sample are consistent with the cosmic γ-ray horizon (*blue filled stars*) as estimated by Domínguez et al. (2011).)

6. Conclusions

This work is a continuation of the photometric redshift determination program utilizing the simultaneous GROND+*Swift*-UVOT data described in Rau et al. (2012) which provided photo-z estimates/limits for hundreds of *Fermi*. We present 40 sources from the 3FGL catalog, for which redshifts (or upper limits) were determined by the photometric technique. Five of these sources are high redshift BL Lacs (z>1.3). The *Fermi* 3LAC catalog comprises of 13 high-z BL Lacs, in addition to the 6 provided by Rau et al. (2012). By including the 5 BL Lacs in this work, the total number of z > 1.3 sources increases to 24, of which 13 are provided by the spectroscopic method and the other 11 by the photometric technique. Therefore, this work increases the sample size of known high-z BL Lacs by ∼30%. It should be noted that ∼50% of the known high-z BL Lacs have been found using the photometric redshift method. The latter method is efficient since obtaining data requires considerably shorter integration time than the spectroscopic method as described in Section 2. Moreover, the properties of these ob-

jects are in agreement with the blazar sequence which were examined using the various parameters as illustrated in Fig. 3, 4 and 5. All the five new sources are classified as LSPs or HSPs exhibiting $L_{sy}^{pk} \simeq 10^{46-48}$ erg s^{-1}. The γ-ray luminosities associated with these objects are $L_\gamma \gtrsim 10^{47}$ erg s^{-1} which are higher than the suggested values in the "Fermi Blazar Divide" introduced by Ghisellini et al. (2009) who divided the FSRQs and BL Lacs on $\Gamma_\gamma - L_\gamma$ plane, such that the BL Lacs show hard spectra ($\Gamma_\gamma < 2.2$) with low γ-ray luminosity ($L_\gamma \lesssim 10^{47}$ erg s^{-1}). Three of these new objects were reported in the 2FHL catalog, from which the highest energy photons (E > 50 GeV) coupled with the redshift measurements were utilized to test the consistency with the currently known EBL models, e.g. Finke et al. (2010); Domínguez et al. (2011); Gilmore et al. (2011). Detecting high-z BL Lacs with substantial amount of > 50 GeV emission allowed us to constrain the EBL in a region where there are not, as yet, measurements of the optical depth. The ones derived here show consistency with the prediction of the EBL model of Domínguez et al. (2011), which is in agreement with the galaxy counts.

Part of the funding for GROND (both hardware as well as personnel) was generously granted from the Leibniz-Prize to Prof. G. Hasinger (DFG grant HA 1850/28-1). AK acknowledges funding under NASA contract NNX15AU67G. The authors acknowledge the *Swift* team and *Swift* PI (N. Gehrels) for scheduling all the *Swift*-UVOT observations.

TABLE 1
TARGET LIST

Name	3FGL Name[a]	$\alpha^{b}_{\rm J2000}$	$\delta^{b}_{\rm J2000}$	$\rm E^{c}_{B-V}$
CGRaBS J0217+0837	J0217.2+0837	02 17 02.66	+08 20 52.4	0.13
PMN J0332−6155	J0331.3−6155	03 31 18.44	−61 55 28.7	0.07
CRATES J0505−1558	J0505.5−1558	05 05 41.57	−15 58 37.9	0.08
SUMSS J052542−601341	J0525.6−6013	05 25 42.43	−60 13 40.4	0.03
TXS 0637−128	J0640.0−1252	06 40 07.01	−12 53 16.1	0.39
GB6 J0708+2241	J0708.9+2239	07 08 58.31	+22 41 35.7	0.05
PMN J0730−6602	J0730.5−6606	07 30 49.42	−66 02 19.3	0.14
1FGLJ0738.2+1741	J0738.1+1741	07 38 07.39	+17 42 18.9	0.03
1RXS J084755.9−070306	J0840.7−0651	08 47 56.71	−07 03 16.5	0.02
PMNJ0842-6053	J0842.0−6055	08 42 26.56	−60 53 50.4	0.21
1FGL J1059.3−1132	J1059.2−1133	10 59 12.60	−11 34 22.1	0.03
1FGL J1107.8+1502	J1107.8+1502	11 07 48.05	+15 02 10.6	0.02
CLASS J1200+0202	J1200.4+0202	12 00 52.9	+12 28 33.2	0.02
PMN J1225−7313	J1225.7−7314	12 25 35.29	−73 13 39.5	0.46
1FGL J1226.7−1332	J1226.9−1329	12 26 54.41	−13 28 38.9	0.04
FRBA J1254+2211	J1254.5+2210	12 54 33.27	+22 11 03.64	0.04
CRATES J1256−1146	J1256.3−1146	12 56 15.95	−11 46 37.4	0.05
SUMSS J132840−472748	J1328.5−4728	13 28 40.64	−47 27 49.3	0.14
PKS 1326−697	J1330.1−7002	13 30 11.07	−70 03 12.9	0.29
FRBA J1338+1153	J1339.0+1153	13 38 58.99	+11 53 17.2	0.03
BZB J1427+2348	J1427.0+2347	14 27 00.39	+23 48 00.0	0.05
1FGL J1521−0350	J1520.8−0348	15 20 49.01	−03 48 51.8	0.10
CGRaBS J1532−1319	J1532.7−1319	15 32 45.37	−13 19 10.1	0.12
CRATES J1552+0850	J1552.1+0852	15 52 03.26	+07 50 47.3	0.04
AT20G J1553−3118	J1553.5−3118	15 53 33.55	−31 18 30.5	0.17
BZB J1555+1111	J1555.7+1111	15 55 43.01	+11 11 24.7	0.05
BZB J1559+2316	J1559.9+2319	15 59 52.20	+23 16 56.6	0.05
CRATES J1610-6649	J1610.8-6649	16 10 46.46	−66 49 01.3	0.09
CGRaBS J1647−6438	J1647.1-6438	16 47 37.74	−64 38 00.27	0.17
CRATES J1918−4111	J1918.2−4110	19 18 16.01	−41 11 30.8	0.09
PKS 1942−313	J1945.9−3115	19 45 59.37	−31 11 38.3	0.07
CRATES J2024−4544	J2022.2−4515	20 22 26.26	−45 13 31.5	0.03
SUMSS J203451−420024	J2034.6−4202	20 34 51.10	−42 00 38.0	0.04
SDSS J20553−00211	J2055.2−0019	20 55 28.23	−00 21 17.2	0.09
PMN J2132−6624	J2131.1−6625	21 32 37.35	−66 24 27.2	0.03
CRATESJ2143-3929	J2143.1−3928	21 43 02.82	−39 29 24.0	0.02
1FGL J2146.6−1345	J2146.6−1344	21 46 37.01	−13 44 00.9	0.04
BZB J2158−3013	J2158.8−3013	21 58 52.03	−30 13 31.4	0.02
PKS 2244−002	J2247.2−0004	22 47 30.19	+00 00 06.5	0.10
BZB J2334+1408	J2334.8+1432	23 34 53.83	+14 32 14.7	0.12

[a] *Fermi*/LAT ID.

[b] Coordinates of the optical counterpart with typical uncertainties of $0\farcs3$ in both directions.

[c] Reddening extracted from Schlafly & Finkbeiner (2011).

TABLE 2
Swift/UVOT PHOTOMETRY

Name	UT Date[a]	AB Magnitude[b]						Δm_{GR-UV}
		$uvw2$	$uvm2$	$uvw1$	u	b	v	mag
CGRaBS J0217+0837	2011−09−13.71	19.51 ± 0.09	19.54 ± 0.14	18.99 ± 0.10	18.34 ± 0.08	17.89 ± 0.09	16.18 ± 0.10	1.07
PMN J0331−6155	2013−06−25.13	19.36 ± 0.10	18.92 ± 0.12	18.99 ± 0.12	18.94 ± 0.16	18.32 ± 0.21	18.18 ± 0.28	−0.18
CRATES J0505−1558	2010−12−08.45	19.32 ± 0.18	19.29 ± 0.25	19.03 ± 0.22	18.87 ± 0.26	18.37 ± 0.28	18.16 ± 0.46	−0.09
SUMSS J052542−601341	2014−02−08.62	22.24 ± 0.28	21.73 ± 0.29	21.31 ± 0.28	> 20.16	19.93 ± 0.30	19.76 ± 0.36	0.71
TXS 0637−128	2014−02−27.63	17.31 ± 0.28	16.88 ± 0.49	17.24 ± 0.28	16.87 ± 0.18	16.72 ± 0.18	16.27 ± 0.32	−0.01
GB6 J0708+2241	2014−02−27.56	17.85 ± 0.11	17.14 ± 0.14	17.27 ± 0.14	17.33 ± 0.14	17.19 ± 0.15	16.34 ± 0.21	0.41
PMN J0730−6602	2014−03−11.03	18.50 ± 0.17	18.20 ± 0.22	18.30 ± 0.24	18.13 ± 0.28	17.33 ± 0.21	16.43 ± 0.18	0.04
1FGL J0738.2+1741	2012−05−22.06	16.88 ± 0.05	16.72 ± 0.08	16.60 ± 0.06	16.25 ± 0.05	15.97 ± 0.06	15.82 ± 0.09	-0.02
PMN J0842-6053	2013−03−21.45	> 21.38	20.58 ± 0.35	20.24 ± 0.29	19.68 ± 0.26	$19.83\pm$	18.30 ± 0.33	0.97
1RXS J084755.9−070306	2013−06−25.47	18.08 ± 0.07	18.00 ± 0.11	17.95 ± 0.10	17.44 ± 0.11	16.97 ± 0.13	16.72 ± 0.21	−0.66
PKS 0944-75	2013-04-13.84	> 20.70	19.46 ± 0.29	19.04 ± 0.19	18.70 ± 0.15	18.39 ± 0.16	17.85 ± 0.24	0.48
1FGL J1059.3−1132	2013−07−25.43	17.75 ± 0.10	17.49 ± 0.11	17.19 ± 0.11	16.74 ± 0.11	16.45 ± 0.14	15.93 ± 0.17	−0.95
1FGL J1107.8+1502	2013−07−17.01	18.40 ± 0.07	18.25 ± 0.09	18.06 ± 0.09	17.67 ± 0.09	17.52 ± 0.13	17.44 ± 0.25	0.11
CLASS J1200+0202	2011−04−22.09	24.19 ± 0.24	24.59 ± 0.55	23.85 ± 0.36	23.92 ± 0.86	> 21.43	> 18.35	2.34
PMN J1225−7313	2013−03−13.58	> 17.78	> 16.59	> 17.53	> 17.94	> 17.68	> 17.26	···
1FGL J1226.7-1332	2012−08−13.97	20.49 ± 0.16	20.06 ± 0.17	20.00 ± 0.22	19.45 ± 0.26	> 19.31	> 18.68	-0.12
FRBA J1254+2211	2011−03−02.13	18.47 ± 0.06	18.44 ± 0.09	18.16 ± 0.08	17.77 ± 0.08	17.43 ± 0.09	17.21 ± 0.13	0.10
CRATES J1256−1146	2011−05−11.11	18.38 ± 0.05	18.18 ± 0.07	17.98 ± 0.06	17.46 ± 0.06	16.58 ± 0.05	15.96 ± 0.05	0.49
SUMSS J132840−472748	2011−02−26.43	18.55 ± 0.13	18.42 ± 0.22	18.22 ± 0.16	17.85 ± 0.15	17.60 ± 0.17	17.19 ± 0.21	−0.23
PKS 1326−697	2014−02−17.45	> 21.46	> 21.86	> 21.02	> 21.01	19.02 ± 0.15	18.02 ± 0.14	2.75
FRBA J1338+1153	2011−05−11.56	20.70 ± 0.13	20.04 ± 0.15	19.85 ± 8.13	19.20 ± 0.12	19.03 ± 0.16	18.98 ± 0.24	1.08
BZB J1427+2348	2014−03−04.47	15.18 ± 0.05	14.98 ± 0.05	14.96 ± 0.05	14.45 ± 0.05	14.25 ± 0.04	13.98 ± 0.04	−0.03
1FGL J1521−0350	2014−01−11.97	19.18 ± 0.13	18.58 ± 0.12	18.37 ± 0.12	17.60 ± 0.10	17.67 ± 0.17	17.10 ± 0.22	−0.50
CGRaBS J1532−1319	2014−04−30.21	> 24.40	> 23.61	> 23.68	> 23.08	> 22.41	> 18.39	3.25
CRATES J1552+0850	2011−09−19.36	20.28 ± 0.26	20.22 ± 0.28	19.54 ± 0.28	19.04 ± 0.29	18.86 ± 0.43	$18.52\pm$	-0.30
AT20G J1553−3118	2013−10−03.68	17.27 ± 0.10	17.16 ± 0.13	16.96 ± 0.11	16.50 ± 0.11	16.37 ± 0.12	16.07 ± 0.17	−0.02
BZB J1555+1111	2014−03−05.46	15.33 ± 0.05	15.13 ± 0.05	15.02 ± 0.05	14.60 ± 0.04	14.36 ± 0.04	14.17 ± 0.05	−0.13
BZB J1559+2316	2014−03−21.07	19.99 ± 0.12	19.79 ± 0.17	19.55 ± 0.15	18.93 ± 0.14	18.51 ± 0.14	18.39 ± 0.25	0.11
CRATES J1610-6649	2013−03−25.22	16.20 ± 0.06	15.90 ± 0.06	15.82 ± 0.06	15.39 ± 0.05	15.23 ± 0.05	15.86 ± 0.07	-0.85
CGRaBS J1647-6438	2013−04−11.98	18.85 ± 0.17	18.68 ± 0.22	18.12 ± 0.15	17.77 ± 0.15	17.38 ± 0.15	17.36 ± 0.18	-0.56
CRATES J1918−4111	2013−09−26.28	21.57 ± 0.36	$20.83\pm$-1	19.49 ± 0.16	18.30 ± 0.10	17.95 ± 0.11	17.41 ± 0.19	0.08
PKS 1942−313	2013−11−23.04	19.41 ± 0.20	19.32 ± 0.28	19.02 ± 0.24	18.37 ± 0.23	17.86 ± 0.26	17.47 ± 0.30	−0.18
CRATES J2024-4544	2012−10−23.01	19.43 ± 0.17	18.91 ± 0.20	18.79 ± 0.19	18.59 ± 0.25	> 18.56	> 18.45	-0.52
SUMSS J203451−420024	2013−09−29.62	18.52 ± 0.76	18.38 ± 0.09	18.45 ± 0.11	18.06 ± 0.14	17.81 ± 0.01	18.10 ± 0.25	−0.04
SDSS J20553-00211	2012−09−29.30	19.08 ± 0.10	19.33 ± 0.17	19.26 ± 0.17	18.86 ± 0.15	18.50 ± 0.17	18.24 ± 0.27	0.09
PMN J2132−6624	2013−07−02.79	> 22.87	> 22.15	> 22.12	> 21.47	> 20.76	> 19.72	···
CRATES J2143-3929	2012−03−19.18	20.38 ± 0.11	19.89 ± 0.16	19.94 ± 0.21	19.90 ± 0.34	19.33 ± 0.41	18.81 ± 0.56	0.02
1FGL J2146.6−1345	2013−04−29.97	17.95 ± 0.05	17.85 ± 0.04	17.70 ± 0.07	17.27 ± 0.07	16.96 ± 0.09	16.96 ± 0.01	−0.19
BZB J2158−3013	2014−03−29.15	15.34 ± 0.03	15.26 ± 0.04	15.24 ± 0.04	14.90 ± 0.03	14.77 ± 0.03	14.56 ± 0.03	0.71
PKS 2244-002	2013−06−17.65	20.29 ± 0.21	19.62 ± 0.21	19.66 ± 0.22	19.09 ± 0.23	18.51 ± 0.24	18.06 ± 0.32	-0.07
BZB J2334+1408	2012−10−15.07	20.79 ± 0.24	> 20.80	20.43 ± 0.30	20.08 ± 0.32	18.93 ± 0.22	> 18.78	0.22

[a] Approximate start time of $uvw2$ exposure.

[b] Corrrected for Galactic foreground reddening. Upper limits are $3\,\sigma$.

[c] Variability-correction factor to be applied to GROND photometry (see text).

TABLE 3
GROND PHOTOMETRY

Name	UT Date[a]	AB Magnitude[b]						
		g'	r'	i'	z'	J	H	K_s
CGRaBS J0217+0837	2011−09−13.38	17.40 ± 0.07	15.31 ± 0.16	15.26 ± 0.10	15.32 ± 0.13	15.23 ± 0.05	14.86 ± 0.05	14.50 ± 0.07
PMN J0331−6155	2013−06−25.42	18.22 ± 0.29	17.67 ± 0.11	···	···	16.57 ± 0.12	16.26 ± 0.05	16.05 ± 0.05
CRATES J0505−1558	2013−11−13.29	18.30 ± 0.14	17.91 ± 0.20	17.07 ± 0.17	17.43 ± 0.38	16.86 ± 0.07	16.42 ± 0.07	16.24 ± 0.08
SUMSS J052542−601341	2014−02−09.12	19.87 ± 0.02	19.48 ± 0.01	19.26 ± 0.04	19.00 ± 0.05	18.40 ± 0.09	17.94 ± 0.10	17.78 ± 0.16
TXS 0637−128	2014−02−27.01	16.67 ± 0.06	16.34 ± 0.06	16.00 ± 0.10	15.83 ± 0.07	15.41 ± 0.07	15.15 ± 0.10	14.97 ± 0.10
GB6 J0708+2241	2015−01−21.10	17.14 ± 0.04	16.81 ± 0.06	16.61 ± 0.05	16.38 ± 0.08	15.75 ± 0.06	15.57 ± 0.07	15.30 ± 0.07
PMN J0730−6602	2014−03−10.99	17.27 ± 0.03	16.89 ± 0.04	16.62 ± 0.04	16.33 ± 0.05	15.93 ± 0.07	15.56 ± 0.09	15.42 ± 0.08
1FGL J0738.2+1741	2012−05−23.69	15.91 ± 0.03	15.61 ± 0.03	15.35 ± 0.03	15.15 ± 0.03	14.79 ± 0.05	14.38 ± 0.05	14.14 ± 0.07
PMN J0842−6053	2012−06−20.95	19.79 ± 0.10	19.58 ± 0.06	19.26 ± 0.08	18.95 ± 0.08	18.46 ± 0.08	18.05 ± 0.08	17.64 ± 0.09
1RXS J084755.9−070306	2014−02−07.16	16.92 ± 0.03	16.60 ± 0.03	16.32 ± 0.05	15.98 ± 0.05	15.68 ± 0.07	15.32 ± 0.08	14.93 ± 0.11
1FGL J1059.3−1132	2014−02−07.20	16.39 ± 0.04	16.01 ± 0.03	15.72 ± 0.04	15.51 ± 0.04	15.08 ± 0.05	14.75 ± 0.08	14.37 ± 0.09
1FGL J1107.8+1502	2013−07−16.96	17.49 ± 0.02	17.28 ± 0.03	17.85 ± 0.05	17.72 ± 0.02	16.73 ± 0.07	16.46 ± 0.12	16.37 ± 0.11
CLASS J1200+0202	2011−11−23.18	21.30 ± 0.10	20.65 ± 0.06	20.54 ± 0.09	20.47 ± 0.11	19.77 ± 0.17	···	···
PMN J1225−7313	2013−03−10.39	18.31 ± 0.03	17.57 ± 0.03	17.16 ± 0.05	16.92 ± 0.04	16.39 ± 0.07	16.02 ± 0.08	15.83 ± 0.09
1FGL J1226.7−1332	2013−06−24.95	19.10 ± 0.10	18.10 ± 0.06	···	17.79 ± 0.10	17.34 ± 0.05	16.98 ± 0.05	16.72 ± 0.07
FRBA J1254+2211	2011−03−04.38	17.38 ± 0.03	17.10 ± 0.03	16.88 ± 0.03	16.68 ± 0.03	16.41 ± 0.05	16.15 ± 0.05	15.80 ± 0.07
CRATES J1256−1146	2014−08−21.97	16.44 ± 0.03	15.62 ± 0.04	15.28 ± 0.03	14.99 ± 0.02	14.63 ± 0.04	14.44 ± 0.04	14.46 ± 0.08
SUMSS J132840−472748	2011−02−28.37	17.58 ± 0.02	17.45 ± 0.01	17.28 ± 0.03	17.09 ± 0.03	16.82 ± 0.08	16.53 ± 0.15	16.45 ± 0.09
PKS 1326−697	2014−02−17.35	18.91 ± 0.04	18.39 ± 0.02	18.22 ± 0.04	17.93 ± 0.06	17.45 ± 0.08	16.86 ± 0.09	16.46 ± 0.15
FRBA J1338+1153	2014−04−22.22	18.98 ± 0.05	18.68 ± 0.03	18.47 ± 0.09	18.28 ± 0.11	17.75 ± 0.09	17.61 ± 0.16	…
BZB J1427+2348	2014−03−01.37	14.21 ± 0.06	13.97 ± 0.05	13.88 ± 0.13	13.56 ± 0.03	13.31 ± 0.06	13.11 ± 0.07	12.86 ± 0.06
1FGL J1521−0350	2014−01−12.35	17.61 ± 0.03	17.25 ± 0.04	17.13 ± 0.04	16.94 ± 0.04	16.65 ± 0.05	16.31 ± 0.08	16.05 ± 0.10
CGRaBS J1532−1319	2014−04−30.37	21.94 ± 0.13	19.95 ± 0.04	18.74 ± 0.03	17.84 ± 0.03	16.20 ± 0.05	15.22 ± 0.05	14.54 ± 0.07
CRATES J1552+0850	2011−09−18.98	18.78 ± 0.03	18.39 ± 0.03	18.06 ± 0.03	17.82 ± 0.03	17.45 ± 0.05	17.02 ± 0.05	16.74 ± 0.07
AT20G J1553−3118	2013−03−19.40	16.35 ± 0.02	16.18 ± 0.01	15.97 ± 0.04	15.88 ± 0.04	15.64 ± 0.07	15.31 ± 0.11	15.09 ± 0.11
BZB J1555+1111	2014−03−05.37	14.32 ± 0.03	14.13 ± 0.03	13.94 ± 0.05	13.77 ± 0.04	13.57 ± 0.07	13.30 ± 0.08	13.10 ± 0.09
BZB J1559+2316	2014−06−03.13	18.44 ± 0.02	18.01 ± 0.01	17.68 ± 0.03	17.37 ± 0.03	16.89 ± 0.06	16.55 ± 0.09	15.92 ± 0.11
CRATES J1610−6649	2013−03−25.34	15.22 ± 0.03	15.23 ± 0.03	14.89 ± 0.03	14.90 ± 0.03	15.18 ± 0.05	14.90 ± 0.05	14.90 ± 0.07
CGRaBS J1647−6438	2014−04−11.98	17.43 ± 0.04	17.76 ± 0.04	17.28 ± 0.04	17.14 ± 0.04	16.96 ± 0.05	16.62 ± 0.05	16.36 ± 0.07
CRATES J1918−4111	2013−09−26.98	17.88 ± 0.02	17.48 ± 0.03	17.20 ± 0.03	16.96 ± 0.06	16.57 ± 0.07	16.27 ± 0.10	15.91 ± 0.07
PKS 1942−313	2013−09−22.98	17.78 ± 0.02	17.29 ± 0.03	16.95 ± 0.03	16.68 ± 0.06	16.17 ± 0.08	15.82 ± 0.12	15.45 ± 0.10
CRATES J2024−4544	2012−10−23.02	18.57 ± 0.04	18.62 ± 0.05	18.28 ± 0.05	18.61 ± 0.05	18.76 ± 0.07	18.90 ± 0.09	18.53 ± 0.10
SUMSS J203451−420024	2013−09−28.99	17.81 ± 0.04	17.76 ± 0.03	17.55 ± 0.06	17.48 ± 0.03	17.28 ± 0.12	17.18 ± 0.17	16.88 ± 0.10
SDSS J20553−00211	2012−09−29.15	18.46 ± 0.03	18.25 ± 0.03	18.06 ± 0.03	17.88 ± 0.03	17.65 ± 0.05	17.57 ± 0.06	17.34 ± 0.07
PMN J2132−6624	2014−11−21.06	20.68 ± 0.05	20.14 ± 0.03	19.94 ± 0.06	19.56 ± 0.07	19.06 ± 0.14	19.15 ± 0.24	18.40 ± 0.20
CRATES J2143−3929	2012−03−19.40	19.15 ± 0.05	18.26 ± 0.07	17.66 ± 0.08	17.75 ± 0.08	17.54 ± 0.05	17.18 ± 0.06	16.89 ± 0.24
1FGL J2146.6−1345	2013−08−26.14	16.93 ± 0.02	16.72 ± 0.01	16.51 ± 0.02	16.34 ± 0.04	16.12 ± 0.06	15.92 ± 0.09	15.69 ± 0.10
BZB J2158−3013	2014−11−09.12	14.73 ± 0.00	14.51 ± 0.03	14.37 ± 0.04	14.20 ± 0.03	13.88 ± 0.07	13.75 ± 0.07	13.50 ± 0.06
PKS 2244-002	2013−06−17.43	18.43 ± 0.03	18.03 ± 0.03	···	···	16.98 ± 0.05	16.63 ± 0.05	16.20 ± 0.07
BZB J2334+1408	2012−10−16.18	18.86 ± 0.03	18.50 ± 0.03	18.27 ± 0.03	18.00 ± 0.03	17.67 ± 0.05	17.46 ± 0.05	17.23 ± 0.07

[a] Exposure start time.

[b] Corrected for Galactic foreground reddening. Not corrected for variability. Upper limits are $3\,\sigma$.

TABLE 4
SED FITTING

Name	$z^a_{\rm phot,best}$	$z^b_{\rm spec,img}$	power law				galaxy			
			$z_{\rm phot}$ [c]	χ^2	P_z^d	β^e	$z_{\rm phot}$ [c]	χ^2	P_z [d]	model
Sources with confirmed photometric redshifts										
SUMSS J052542-601341	$1.78^{+0.16}_{-0.13}$	···	$1.78^{+0.16}_{-0.13}$	10.4	98.9	1.25	$0.02^{+0.03}_{-0.02}$	54.7	99.9	Spi4_template_norm.sed
FRBA J1338+1153	$1.49^{+0.15}_{-0.14}$	> 1.587	$1.49^{+0.15}_{-0.14}$	3.7	98.8	1.05	$1.27^{+0.06}_{-1.27}$	27.2	77.5	I22491_60_TQSO1_40.sed
1FGL J1521.0−0350	$1.46^{+0.12}_{-0.11}$	>0.867	$1.46^{+0.12}_{-0.11}$	7.6	99.7	0.90	$1.19^{+0.28}_{-0.05}$	27.0	81.8	I22491_40_TQSO1_60.sed
CRATES J1918−4111	$2.16^{+0.11}_{-0.01}$	> 1.591	$2.16^{+0.11}_{-0.01}$	5.6	100.0	1.20	$0.00^{+0.01}_{-0.00}$	128.0	100.0	S0_90_QSO2_10.sed
1FGL J2146.6−1345	$1.34^{+0.11}_{-0.20}$	···	$1.34^{+0.11}_{-0.20}$	15.1	93.5	0.75	$1.45^{+0.05}_{-0.03}$	39.2	100.0	pl_I22491_20_TQSO1_80.sed
Sources with photometric redshifts upper limits										
CGRaBS J0217+0837	···	0.085	$1.47^{+0.01}_{-0.06}$	153.49	82.88	1.90	$0.22^{+0.02}_{-0.01}$	95.72	99.87	M82_template_norm.sed
PMN J0331-6155	< 1.15	···	$0.03^{+1.12}_{-0.03}$	14.7	13.3	1.35	$0.41^{+0.22}_{-0.10}$	6.9	76.3	Sey18_template_norm.sed
CRATES J0505-1558	< 1.25	···	$0.02^{+1.23}_{-0.02}$	08.3	10.4	1.25	$0.46^{+0.13}_{-0.44}$	13.5	52.9	I22491_90_TQSO1_10.sed
TXS 0637-128	< 1.29	···	$0.02^{+1.27}_{-0.02}$	4.7	10.5	1.05	$0.46^{+0.46}_{-0.44}$	3.6	34.5	I22491_50_TQSO1_50.sed
GB6 J0708+2241	···	···	$0.03^{+0.99}_{-0.03}$	34.4	16.0	1.10	$0.88^{+0.08}_{-0.09}$	10.6	99.7	I22491_50_TQSO1_50.sed
PMN J0730-6602	<1.35	···	$1.07^{+0.28}_{-1.07}$	15.4	34.9	1.20	$0.05^{+0.03}_{-0.04}$	18.1	99.9	I22491_80_TQSO1_20.sed
1FGL J0738.2+1741	< 1.01	0.424	$0.38^{+0.63}_{-0.38}$	5.07	26.58	1.05	$0.00^{+0.03}_{-0.00}$	13.38	100.00	I22491_40_TQSO1_60.sed
PMNJ0842−6053	< 1.38	···	$1.16^{+0.22}_{-0.11}$	16.63	60.72	1.35	$1.17^{+0.08}_{-0.04}$	8.13	100.00	I22491_70_TQSO1_30.sed
1RXS J084755.9-070306	< 1.23	···	$0.96^{+0.27}_{-0.96}$	9.8	34.7	1.20	$0.02^{+0.04}_{-0.02}$	17.8	99.9	I22491_70_TQSO1_30.sed
1FGL J1059.3−1132	< 1.37	···	$1.22^{+0.15}_{-0.27}$	01.9	63.6	1.20	$0.04^{+0.04}_{-0.04}$	28.8	99.9	I22491_70_TQSO1_30.sed
1FGL J1107.8+1502	···	···	$1.73^{+0.10}_{-0.07}$	250.4	100.0	2.15	$0.63^{+0.03}_{-0.03}$	175.0	99.7	pl_QSOH_template_norm.sed
CLASS J1200+0202	···	···	$3.13^{+0.11}_{-0.06}$	23.53	99.36	0.75	$3.03^{+0.02}_{-0.04}$	22.66	95.38	pl_QSOH_template_norm.sed
PMN J1225−7313	···	···	$2.27^{+0.06}_{-2.27}$	40.0	22.3	1.55	$0.49^{+0.06}_{-0.07}$	3.7	99.7	I22491_template_norm.sed.save
1FGL J1226.7−1332	···	0.456	$0.00^{+0.94}_{-0.00}$	90.38	10.32	1.70	$0.44^{+0.01}_{-0.01}$	15.69	99.97	Spi4_template_norm.sed
FRBA J1254+2211	< 1.39	0.386	$1.23^{+0.16}_{-0.11}$	9.11	77.20	0.95	$0.00^{+0.00}_{-0.01}$	30.32	100.00	I22491_50_TQSO1_50.sed
CRATES J1256−1146	···	0.058	$1.28^{+0.02}_{-0.02}$	388.9	100.0	1.55	$0.08^{+0.02}_{-0.02}$	28.5	100.0	M82_template_norm.sed
PKS 1326-697	···	···	$3.06^{+0.03}_{-0.01}$	37.8	100.0	1.10	$2.73^{+0.05}_{-0.01}$	45.1	98.8	Spi4_template_norm.sed
SUMSS J132840-472748	< 1.44	···	$1.26^{+0.18}_{-0.33}$	21.3	65.4	0.65	$1.53^{+0.02}_{-0.04}$	23.7	91.9	pl_I22491_20_TQSO1_80.sed
BZB J1427+2348	< 0.86	···	$0.85^{+0.01}_{-0.85}$	09.2	29.3	0.85	$0.05^{+0.23}_{-0.05}$	41.7	61.6	I22491_40_TQSO1_60.sed
CGRaBS J1532−1319	···	···	$4.00^{+0.00}_{-0.00}$	1384.56	100.00	1.50	$1.69^{+0.01}_{-0.01}$	291.08	100.00	S0_90_QSO2_10.sed
CRATESJ1552+0850	< 1.54	1.05	$1.43^{+0.11}_{-0.18}$	4.59	66.00	1.25	$0.00^{+0.00}_{-0.00}$	46.92	54.94	I22491_70_TQSO1_30.sed
AT20G J1553−3118	< 1.23	···	$1.23^{+0.20}_{-0.26}$	10.3	75.2	0.70	$1.50^{+0.04}_{-0.07}$	17.3	99.8	pl_I22491_20_TQSO1_80.sed
BZB J1555+1111	< 0.95	···	$0.93^{+0.02}_{-0.33}$	10.1	42.3	0.80	$0.24^{+0.01}_{-0.21}$	68.1	37.4	pl_I22491_20_TQSO1_80.sed
BZB J1559+2316	< 1.43	···	$1.18^{+0.25}_{-0.43}$	9.6	56.1	1.45	$0.03^{+0.03}_{-0.01}$	56.7	100.0	I22491_template_norm.sed.save
CRATES J1610−6649	···	···	$1.53^{+0.02}_{-0.07}$	129.86	99.94	0.25	$1.54^{+0.06}_{-0.00}$	188.92	97.54	pl_QSOH_template_norm.sed
CGRaBS J1647−6438	···	···	$1.33^{+0.11}_{-0.18}$	119.07	66.93	0.75	$1.72^{+0.01}_{-0.02}$	73.04	100.00	pl_I22491_30_TQSO1_70.sed
PKS 1942−313	< 1.63	···	$1.38^{+0.25}_{-0.34}$	4.2	68.9	1.45	$0.07^{+0.02}_{-0.03}$	37.7	100.0	I22491_template_norm.sed.save
CRATESJ2024−4544	< 1.60	···	$1.53^{+0.07}_{-0.08}$	43.35	99.75	2.05	$1.10^{+0.02}_{-0.01}$	152.12	99.59	pl_QSOH_template_norm.sed
SUMSS J203451-420024	···	···	$1.26^{+0.20}_{-1.26}$	12.7	36.0	0.55	$0.49^{+0.06}_{-0.07}$	18.9	66.9	pl_TQSO1_template_norm.sed
SDSSJ20553−00211	< 1.15	0.407	$0.96^{+0.19}_{-0.96}$	15.94	34.04	0.70	$0.46^{+0.01}_{-0.01}$	54.89	91.46	pl_I22491_20_TQSO1_80.sed
PMN J2132-6624	···	···	$2.63^{+0.32}_{-0.09}$	6.1	96.6	1.25	$0.00^{+0.04}_{-0.00}$	14.0	99.9	M82_template_norm.sed
CRATESJ2143−3929	···	0.429	$0.93^{+0.26}_{-0.93}$	64.78	31.60	1.40	$0.31^{+0.03}_{-0.03}$	20.84	99.60	Spi4_template_norm.sed
BZB J2158−3013	< 1.07	0.116	$0.03^{+1.04}_{-0.03}$	04.1	14.4	0.70	$0.87^{+0.04}_{-0.09}$	21.2	96.5	pl_I22491_20_TQSO1_80.sed
PKS2244−002	< 1.53	0.949	$1.40^{+0.13}_{-0.11}$	5.42	92.50	1.35	$1.29^{+0.03}_{-0.04}$	67.49	96.66	I22491_70_TQSO1_30.sed
BZBJ2334+1408	···	0.415	$1.71^{+0.12}_{-0.05}$	133.84	92.01	1.35	$0.04^{+0.00}_{-0.00}$	142.54	100.00	M82_template_norm.sed

[a] Best photometric redshift.

[b] Spectroscopic redshift, if known.

[c] Photometric redshifts with 2σ confidence level

[d] Redshift probability density at $z_{phot} \pm 0.1(1 + z_{phot})$

[e] Spectral slope for power law model of the form $F_\lambda \propto \lambda^{-\beta}$

REFERENCES

Abdo, A. A., Ackermann, M., Ajello, M., et al. 2009, The Astrophysical Journal, 700, 597

—. 2010, The Astrophysical Journal, 723, 1082

Acero, F., Ackermann, M., Ajello, M., et al. 2015, The Astrophysical Journal Supplement Series, 218, 23

Ackermann, M., Ajello, M., Allafort, A., et al. 2012, Science (New York, N.Y.), 338, 1190

—. 2013, The Astrophysical Journal Supplement Series, 209, 34

Ackermann, M., Ajello, M., Atwood, W. B., et al. 2015, The Astrophysical Journal, 810, 14

—. 2016, The Astrophysical Journal Supplement Series, 222, 5

Aharonian, F., Akhperjanian, A. G., Bazer-Bachi, A. R., et al. 2006, Nature, 440, 1018

Aihara, H., Allende Prieto, C., An, D., et al. 2011, The Astrophysical Journal Supplement Series, 193, 29

Ajello, M., Shaw, M. S., Romani, R. W., et al. 2012, The Astrophysical Journal, 751, 108

Arnouts, S., Cristiani, S., Moscardini, L., et al. 1999, Monthly Notices of the Royal Astronomical Society, 310, 540

Blandford, R. D., & Rees, M. J. 1978, Physica Scripta, 17, 265

Bohlin, R. C., Colina, L., & Finley, D. S. 1995, The Astronomical Journal, 110, 1316

Chabrier, G., Baraffe, I., Allard, F., & Hauschildt, P. 2000, The Astrophysical Journal, 542, 464

Domínguez, A., & Ajello, M. 2015, The Astrophysical Journal, 813, arXiv:1510.07913

Domínguez, A., Finke, J. D., Prada, F., et al. 2013, The Astrophysical Journal, 770, 77

Domínguez, A., Primack, J. R., Rosario, D. J., et al. 2011, Monthly Notices of the Royal Astronomical Society, 410, 2556

Finke, J. D. 2013, The Astrophysical Journal, 763, 134

Finke, J. D., Razzaque, S., & Dermer, C. D. 2010, The Astrophysical Journal, 712, 238

Fossati, G., Maraschi, L., Celotti, A., Comastri, A., & Ghisellini, G. 1998, Monthly Notices of the Royal Astronomical Society, 299, 433

Gehrels, N., Chincarini, G., Giommi, P., et al. 2004, The Astrophysical Journal, 611, 1005

Ghisellini, G., Celotti, A., Fossati, G., Maraschi, L., & Comastri, A. 1998, Monthly Notices of the Royal Astronomical Society, 301, 451

Ghisellini, G., Maraschi, L., & Tavecchio, F. 2009, Monthly Notices of the Royal Astronomical Society: Letters, 396, L105

Ghisellini, G., Tavecchio, F., Foschini, L., et al. 2012, Monthly Notices of the Royal Astronomical Society, 425, 1371

Gilmore, R. C., Somerville, R. S., Primack, J. R., & Domínguez, A. 2011, Monthly Notices of the Royal Astronomical Society, Volume 422, Issue 4, pp. 3189-3207., 422, 3189

Greiner, J., Bornemann, W., Clemens, C., et al. 2008, Publications of the Astronomical Society of the Pacific, 120, 405

Hartman, R. C., Bertsch, D. L., Bloom, S. D., et al. 1999, THE ASTROPHYSICAL JOURNAL SUPPLEMENT SERIES, 123, 79

Ilbert, O., Arnouts, S., McCracken, H. J., et al. 2006, Astronomy and Astrophysics, 457, 841

Kataoka, J., Madejski, G., Sikora, M., et al. 2008, The Astrophysical Journal, 672, 787

Krühler, T., Küpcü Yolda, A., Greiner, J., et al. 2008, The Astrophysical Journal, 685, 376

Krühler, T., Schady, P., Greiner, J., et al. 2011, Astronomy & Astrophysics, 526, A153

Maraschi, L., Fossati, G., Tagliaferri, G., & Treves, A. 1995, The Astrophysical Journal, 443, 578

Maraschi, ., Ghisellini, ., & Celotti, . 1994, IAU Symposium No. 159: Multi-wavelength continuum emission of AGN

Padovani, P., Giommi, P., & Rau, A. 2012, Monthly Notices of the Royal Astronomical Society: Letters, 422, L48

Pickles, A. 1998, Publications of the Astronomical Society of the Pacific, 110, 863

Poole, T. S., Breeveld, A. A., Page, M. J., et al. 2007, Monthly Notices of the Royal Astronomical Society, 383, 627

Rau, A., Schady, P., Greiner, J., et al. 2012, Astronomy & Astrophysics, 538, A26

Roming, P. W. A., Kennedy, T. E., Mason, K. O., et al. 2005, Space Science Reviews, 120, 95

Ryabinkov, A. I., Kaminker, A. D., & Varshalovich, D. A. 2003, Astronomy and Astrophysics, 412, 707

Salvato, M., Hasinger, G., Ilbert, O., et al. 2009, The Astrophysical Journal, 690, 1250

Salvato, M., Ilbert, O., Hasinger, G., et al. 2011, The Astrophysical Journal, 742, 61

Sambruna, R. M., Maraschi, L., & Urry, C. M. 1996, The Astrophysical Journal, 463, 444

Sbarrato, T., Ghisellini, G., Maraschi, L., & Colpi, M. 2012, Monthly Notices of the Royal Astronomical Society, 421, 1764

Schlafly, E. F., & Finkbeiner, D. P. 2011, The Astrophysical Journal, 737, 103

Shaw, M. S., Romani, R. W., Cotter, G., et al. 2013, The Astrophysical Journal, 764, 135

Skrutskie, M. F., Cutri, R. M., Stiening, R., et al. 2006, The Astronomical Journal, 131, 1163

Stecker, F. W., de Jager, O. C., & Salamon, M. H. 1992, The Astrophysical Journal, 390, L49

Urry, C. M., & Padovani, P. 1995, Publications of the Astronomical Society of the Pacific, 107, 803

Venters, T. M., & Pavlidou, V. 2007, in AIP Conference Proceedings, Vol. 921, 163–165

This 2-column preprint was prepared with the AAS LaTeX macros v5.2.